Phase diagram and scaling behavior of fluid vesicles

G. Gompper[1] and D.M. Kroll[2]
[1]*Sektion Physik der Ludwig-Maximilians-Universität München, Theresienstrasse 37, 80333 München, Germany*
[2]*Department of Medicinal Chemistry and Minnesota Supercomputer Institute, University of Minnesota, 308 Harvard Street SE, Minneapolis, Minnesota 55455*
(Received 15 July 1994)

The phase diagram and the scaling behavior of self-avoiding fluid vesicles as a function of the bending rigidity κ and the pressure increment Δp is studied using Monte Carlo simulations and scaling arguments. For $\Delta p > 0$, a line of first-order transitions is observed between a branched-polymer-like phase and an inflated phase. The scaling behavior in the inflated phase along this line seems to be characterized by a universal exponent $\nu \simeq 0.8$. The first-order line ends at small positive Δp; it extends to negative Δp as a line of compressibility maxima. For $\Delta p < 0$, this line can be understood as a line of buckling transitions. For even more negative Δp and sufficiently large κ, stomatocytes are stable. We present evidence for the absence of a phase transition as a function of κ at $\Delta p = 0$ by showing that the volume V of a N-monomer vesicle scales as $\langle V \rangle = N^{3/2}\Theta_V(\sqrt{N}/\xi_p)$, with a smooth scaling function Θ_V. The exponential κ dependence of the persistence length ξ_p is found to be in excellent agreement with renormalization group results.

PACS number(s): 05.40.+j, 64.60.Fr, 87.22.Bt

I. INTRODUCTION

The thermal behavior of membranes and vesicles has recently attracted a great deal of attention [1–3]. Membranes are (approximately) incompressible two-dimensional films composed of amphiphiles or lipids which—on experimentally relevant time scales—do not change their area. For this reason, the shape and fluctuations of membranes are controlled by their bending rigidity [4–6] rather than by a surface tension as is the case for interfaces. For bilayer membranes, which do not have a preferred radius of curvature, the curvature elastic energy has the form [5]

$$\mathcal{H}/(k_BT) = \int dS\ [2\kappa H^2 + \bar{\kappa}K]\ , \qquad (1)$$

with bending rigidity κ and saddle-splay modulus $\bar{\kappa}$, where H is the mean curvature and K the Gaussian curvature. Theoretical and experimental work on vesicles has been restricted almost exclusively to the very-large-bending-rigidity regime, where thermal fluctuations are of only minor importance [7]. Very little is known, however, about the behavior of vesicles in the low-bending-rigidity regime.

The two intensive thermodynamic fields that determine the conformation and structure of vesicles are the bending rigidity κ and the pressure difference $\Delta p = p_{in} - p_{out}$ between the vesicle interior and exterior. Δp is the thermodynamic variable conjugate to the enclosed volume V. The behavior of self-avoiding low-bending-rigidity vesicles has been studied theoretically as a function of κ for $\Delta p = 0$ [8–10], and as a function of Δp for $\kappa = 0$ [11–15]. In the first case, a peak in the specific heat is observed at $\kappa \simeq 1$. The interpretation of this peak is the subject of intense current debate [8,16–18], and it is still an open question whether there is a phase transition separating a low-bending-rigidity, branched-polymer-like phase [8,9,19,20] from a high-bending-rigidity, extended phase. For $\kappa = 0$, a first-order transition is observed between a low-pressure, branched-polymer-like phase and a high-pressure, inflated phase [11]. Experimentally, low-bending-rigidity vesicles have been shown to be able to penetrate through the intact skin [21], and may thus have a large number of applications in medicine, biotechnology, and other areas.

In this paper, we present the results of an extensive Monte Carlo simulation study of the phase diagram of fluid vesicles as a function of the bending rigidity κ and (positive and negative) pressure increment Δp.

II. CURVATURE MODEL

The model we study consists of N hard spheres of diameter $\sigma_0 = 1$ which are connected by flexible tethers of length $\ell_0 < \sqrt{3}\sigma_0$ to form a two-dimensional network of spherical topology. ℓ_0 is chosen to ensure self-avoidance. In our simulations, we have used both $\ell_0 = \sqrt{2.8}$ and $\ell_0 = \sqrt{2.0}$. In order to allow for diffusion within the membrane, and thus to describe fluid membranes, tethers can be cut and reattached between the four beads that form two neighboring triangles [22,23]. A Monte Carlo step (MCS) then consists of an attempt to update the positions of all N beads by a random increment in the cube $[-s, s]^3$, followed by N attempted tether cuts. We chose $s = 0.15$ for $\ell_0 = \sqrt{2.8}$ and $s = 0.10$ for $\ell_0 = \sqrt{2.0}$ so that approximately 50% of the attempted coordinate updates were successful. Averages are typically calculated over runs from 20 to 100 million MCS. In the rest of this paper we employ the dimensionless pressure increment $p = \Delta p\sigma_0^3/k_BT$ and measure the volume in units

of σ_0^3.

The bending elastic energy we employ is [24]

$$\mathcal{H}/(k_BT) = \lambda \sum_{\langle ij \rangle} (1 - \mathbf{n}_i \cdot \mathbf{n}_j) , \tag{2}$$

where $\mathbf{n}_i$ is the unit normal vector of triangle i, and the sum runs over all pairs of neighboring triangles. In the continuum limit [25],

$$\lambda \sum_{\langle ij \rangle} (1 - \mathbf{n}_i \cdot \mathbf{n}_j) \simeq \int dS \, [2\kappa H^2 - \kappa K] \tag{3}$$

so that for our choice of bending energy (2), $\bar{\kappa} = -\kappa$. The relationship between the coupling constant λ in (2) and the bending rigidity κ can be determined by covering a sphere of radius R with equilateral triangles of side ℓ and taking the limit $R \to \infty$. In this way we find

$$\kappa = -\bar{\kappa} = \lambda/\sqrt{3} . \tag{4}$$

For compatibility with our earlier work [8,11] we use the measure

$$\prod_i d\mathbf{r}_i (q_i/3)^{3/2} , \tag{5}$$

where $\mathbf{r}_i$ is the three-dimensional coordinate vector of vertex i, and q_i its coordination number. A comparison of the results of Ref. [11] with those of Ref. [12], where the factor $(q_i/3)^{3/2}$ has been omitted, shows that the extra contribution in the measure has no noticeable effect.

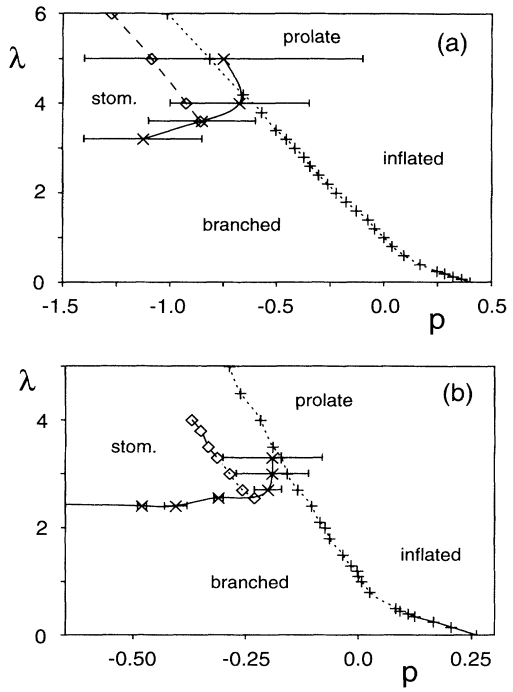

FIG. 1. Phase diagram of fluid vesicles as a function of pressure increment p and bending rigidity λ, for (a) $N = 127$ and (b) $N = 247$. First-order transitions are denoted by solid lines, compressibility maxima by dotted lines. The dumbbell-metastable discocyte transitions are shown as a dashed line. The error bars span the spinodals for the transition to stomatocytes. The solid line through their midpoints serves as a guide to the eye.

III. PHASE DIAGRAM

The λ-p phase diagrams for systems consisting of $N = 127$ and $N = 247$ beads are shown in Fig. 1. The first-order transition observed previously [11] at $\lambda = 0$ persists to finite values of λ. With increasing λ, the transition occurs at lower and lower values of p, since both the bending rigidity and the (positive) pressure act to increase the volume of the vesicle. This first-order transition is characterized by a bimodal probability distribution function $P(V)$ for the volume. We locate the transition at the point at which the two maxima of $P(V)$ are of equal height. These maxima approach each other with increasing λ, and merge into a single peak at $\lambda \simeq 0.32$ for $N = 127$, $\lambda \simeq 0.45$ for $N = 247$, and $\lambda \simeq 0.52$ for $N = 407$. Thus, the line of first-order transitions extends to higher values of λ for larger system sizes. For values of λ beyond this "critical" point, we find a line of maxima of the compressibility

$$\chi = \frac{1}{\langle V \rangle} \frac{\partial}{\partial p} \langle V \rangle . \tag{6}$$

This line extends to the highest values of λ studied in this paper, $\lambda = 6$. It crosses the λ axis at $\lambda \simeq 1.0$ for $N = 127$ and $\lambda \simeq 1.2$ for $N = 247$. For larger λ, there is a rapid change in the vesicle shape, from roughly spherical prolate to dumbbell, as this line of compressibility maxima is crossed with decreasing p. A few typical configurations are shown in Fig. 2.

The phase diagram (in the pressure ensemble) as a function of λ and the reduced volume $\tilde{v} = v_0^{-1} \langle V \rangle (N - 2)^{-3/2}$ is shown in Fig. 3. Here, $v_0^{-1} = 3^{1/4} 2^{5/2} \pi^{1/2} \langle \ell \rangle^{-3}$ is a constant, and $\langle \ell \rangle \simeq 1.35$ is the average distance between neighboring beads [26]. The phase diagram in the *volume* ensemble should be rather similar. All coexistence regions shrink to single lines in this case, since the volume in both phases has to be identical at coexistence. These lines must be located somewhere inside the two-phase coexistence regions of Fig. 3.

The large-κ portion of our phase diagram differs from that obtained by minimizing the bending energy in the pressure ensemble [27], where only a single transition from spheres to prolates is found with decreasing $p < 0$. In this ensemble, stable non-self-intersecting $T = 0$ configurations cease to exist before other phase transitions can occur. We find much better agreement with the $T = 0$ analysis of vesicle shapes in the volume ensemble [28], where a transition from stomatocytes to discocytes occurs at a reduced volume $v \equiv V/V_{sphere} = 0.59 = v^{(1)}$, and a transition from discocytes to dumbbells at $v = 0.65 = v^{(2)}$. Our simulation results indicate that the discocyte-prolate transition occurs at $0.45 < \tilde{v}^{(2)} < 0.52$

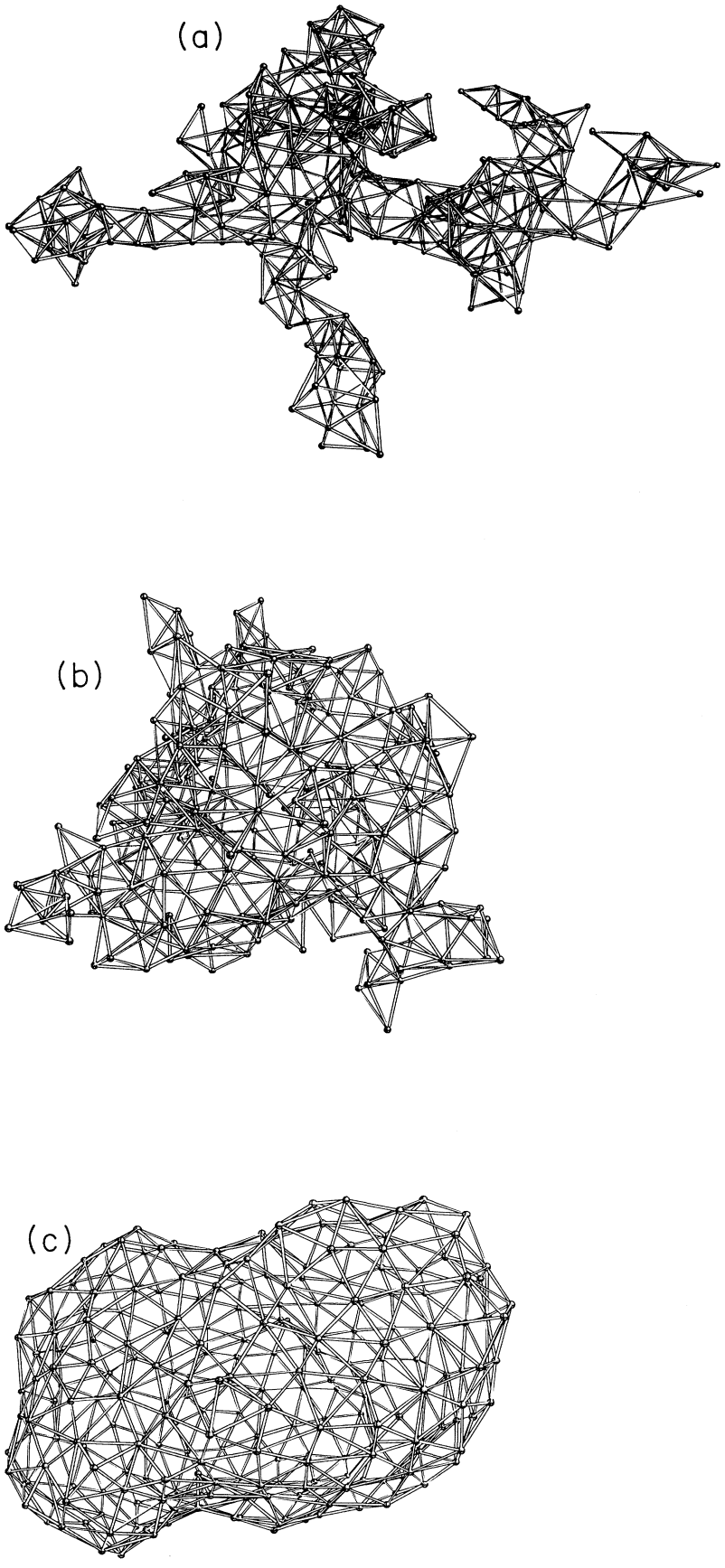

FIG. 2. Typical configurations of vesicles with $N = 247$ monomers. (a) $\lambda = 0.35$, $p = 0.125$ (branched polymer), (b) $\lambda = 0.35$, $p = 0.125$ (inflated), (c) $\lambda = 2.0$, $p = -0.05$ (prolate), (d) $\lambda = 2.4$, $p = -0.19$ (dumbbell), (e) $\lambda = 2.4$, $p = -0.35$ (branched polymer), (f) $\lambda = 3.0$, $p = -0.27$ (stomatocyte), (g) $\lambda = 3.8$, $p = -0.35$ (discocyte).

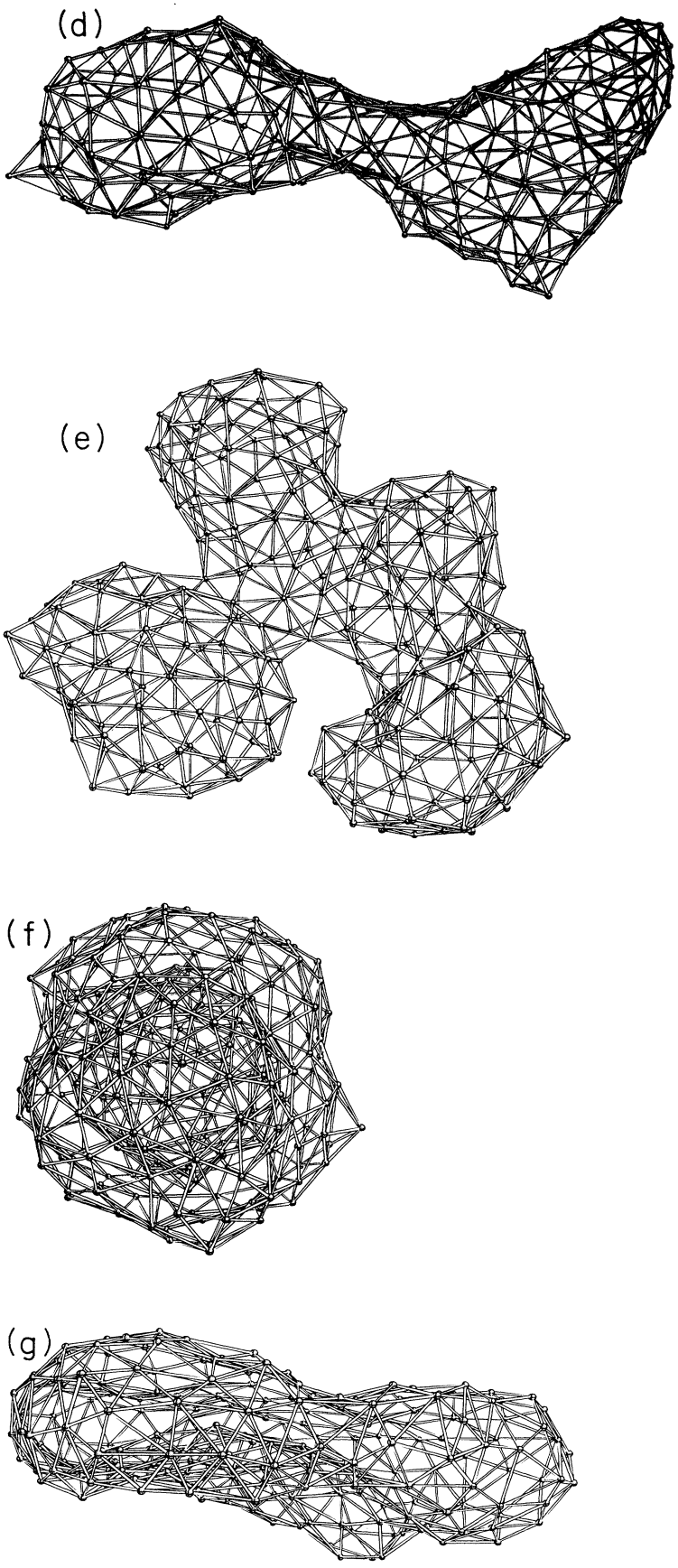

FIG. 2 *(Continued).*

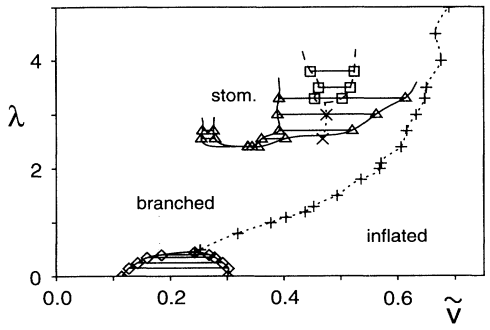

FIG. 3. Phase diagram of fluid vesicles in the pressure ensemble, as a function of reduced average volume $\tilde{v} = v_0^{-1}\langle V\rangle(N-2)^{-2/3}$, with $v_0^{-1} = 3^{1/4}2^{5/2}\pi^{1/2}\langle\ell\rangle^{-3}$, and bending rigidity λ, for $N = 247$. Compressibility maxima are denoted by dotted lines, the dumbbell-metastable discocyte transitions by a dashed line. The solid line in Fig. 1(b) has been used to estimate the average volume $\langle V\rangle$ at the transition to stomatocytes.

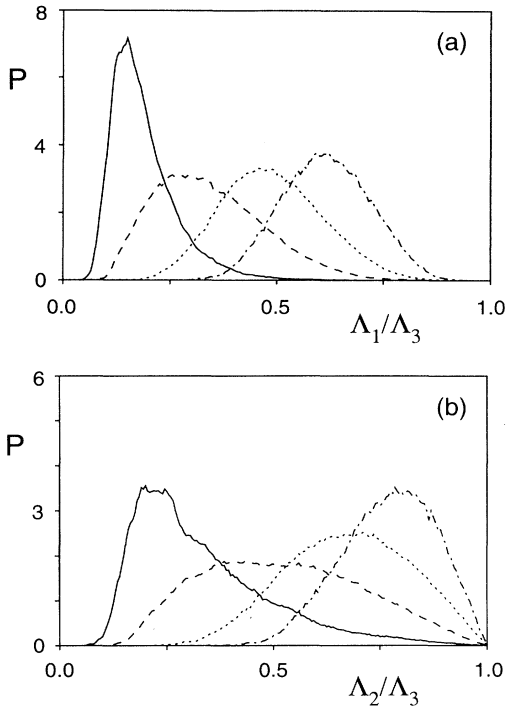

FIG. 4. The probability distribution $P(\Lambda_i/\Lambda_3)$ of the moments of inertia, for $N = 247$, $\ell_0 = \sqrt{2.8}$, $\lambda = 2.0$, and $p = 0.10$ (dashed-dotted lines), $p = 0$ (dotted lines), $p = -0.05$ (dashed lines), and $p = -0.10$ (solid lines). (a) $P(\Lambda_1/\Lambda_3)$, (b) $P(\Lambda_2/\Lambda_3)$.

for the values of λ studied, see Fig. 3. In general, we expect transitions to be shifted to smaller values of the reduced volume—compared to the $T = 0$ results—since thermal fluctuations reduce $\langle V\rangle$, while $\tilde{v}$ is defined with respect to the volume of a *rigid* sphere (of equal area). The good agreement between our results and the phase diagram obtained by minimizing the bending energy in the volume ensemble is due to the fact that the effects of both self-avoidance and thermal fluctuations are included in our analysis.

In order to characterize the shape of the vesicles, we have studied the eigenvalues $\Lambda_1 < \Lambda_2 < \Lambda_3$ of the moment of inertia tensor,

$$\mathcal{T}_{\alpha,\beta} = \frac{1}{2N^2}\sum_{i,j}\frac{q_i}{6}\frac{q_j}{6}[r_i^\alpha - r_j^\alpha][r_i^\beta - r_j^\beta], \qquad (7)$$

where $\mathbf{r}_i$ is the position of monomer i, and q_i is its coordination number. The probability distributions of the anisotropies Λ_1/Λ_3 and Λ_2/Λ_3 are shown in Fig. 4 for $\lambda = 2.0$ and four values of p in the vicinity of the line of maximum compressibility. Note that for all pressures shown, the distributions $P(\Lambda_i/\Lambda_3)$ are very broad, indicating enormous shape fluctuations. With decreasing pressure, the average shape changes from spherical prolate to dumbbell, as mentioned above.

For large λ and sufficiently *negative* pressures, stomatocytes are found to be stable. Stomatocytes decay with increasing pressure into dumbbells, and with decreasing λ into branched-polymer-like shapes. The transition at large λ is strongly first order, and, therefore, cannot be localized easily. The error bars shown in Fig. 1 span the spinodal lines. Stomatocytes are also unstable at large negative pressures with respect to flat, pancake-shaped configurations since the latter have a smaller volume in our model. In the limit of very large negative pressures these pancakes transform smoothly into branched-polymer-like configurations. The lowest value of λ for which stomatocytes are stable is $\lambda \simeq 3.1$ for $N = 127$ and $\lambda \simeq 2.4$ for $N = 247$. The region of stability of stomatocytes, therefore, extends to *smaller* values of λ for larger system sizes.

We also see discocytes, but it appears that they are only metastable, and always decay into stomatocytes. Nevertheless, we do observe a transition between discocytes and prolate, dumbbell-shaped vesicles. There is a line of first-order transitions between these two phases for large λ, which ends in a *lower* critical point. There is also a line of maxima in the compressibility at lower values of λ; however, it is very short and never approaches the line of compressibility maxima mentioned above. In this case, the "critical" point occurs at $\lambda \simeq 3.5$ for $N = 127$ and $\lambda \simeq 3.3$ for $N = 247$, i.e., the critical point moves to lower λ with increasing system size.

It should be emphasized that there is a fundamental difference between the "phase transitions" for small λ (i.e., the transition between the branched-polymer phase and the inflated phase) and for large λ (i.e., the transition between prolates and stomatocytes). In the former case, a true first-order transition occurs in the thermodynamic limit $N \to \infty$. This can be seen by studying the volume distribution function $P(V)$ as a function of the vesicle area; with increasing N, the bimodal structure becomes more pronounced [11]. In the latter case, the energy barrier between the two coexisting shapes remains finite even for $N \to \infty$ because the bending energy

is scale invariant [29]. This implies that there is a finite probability for a vesicle to jump between the two minima of the free energy, independent of the system size. In our simulations, we see an indication that this is indeed the case because the number of MCS it takes for a vesicle of $N = 127$ monomers to jump from a prolate shape to a stomatocyte is roughly the same as for a vesicle of $N = 247$ monomers.

IV. SCALING BEHAVIOR FOR p=0

The behavior of membranes as a function of the bending rigidity κ has been discussed intensively in recent years. In many studies of membranes, both with and without self-avoidance, the specific heat has been found to have a peak near $\lambda = 1$. The location of this peak has been interpreted either as a second-order phase transition between a crumpled, small-κ phase, and an extended phase at large bending rigidities [17,30–35], or as the point at which the persistence length [36] reaches the system size [8]. Both of these interpretations seem to be incorrect. It has been shown in Refs. [16] and [17] for vesicles without self-avoidance that the peak in the specific heat stops growing with system size for sufficiently large N, and that the location of the peak becomes independent of N. It has also been demonstrated in Ref. [16] that the specific heat of the two-dimensional Heisenberg model, where the absence of a phase transition can be proven exactly, shows a very similar behavior. The specific heat is, therefore, not a good quantity to analyze when studying the phase behavior of membranes as a function of κ.

A valuable guide for understanding the scaling behavior of vesicles is the scaling analysis of ring polymers in two dimensions [37–40]. In particular, it has been shown [40] that the area A enclosed by the ring polymer in two dimensions scales as

$$\langle A\rangle_{ring} = A_\infty N^2 \Theta_A(N/\kappa) \ , \tag{8}$$

where N is the number of monomers in the ring. For large N,

$$\Theta_A(y) \sim y^{-2(1-\nu)} \ , \tag{9}$$

where $\nu = 3/4$ is the self-avoiding random walk exponent in $d = 2$. Thus, for small κ, $\langle A\rangle_{ring} \sim N^{2\nu}$, as expected.

Let us try now the same scaling ansatz for vesicles. To do so, note that the scaling variable in Eq. (8) is the ratio of the radius R_{ring} of a large-κ ring polymer and the persistence length $\xi_p(ring)$. We assume that the scaling variable in the case of vesicles is the same ratio of length scales, R/ξ_p. For ring polymers, one has $R_{ring} \sim N$ and $\xi_p(ring) \sim \kappa$, while for vesicles, $R_{ves} \sim \sqrt{N}$, and [41–43]

$$\xi_p(ves) = a_0(\ell_0) \ \exp\left(\frac{4\pi}{3}\kappa\right) \ . \tag{10}$$

Thus, the volume should scale as

$$\langle V\rangle = V_\infty N^{3/2} \Theta_V(y) \tag{11}$$

with

$$y = y_0(\ell_0)\sqrt{N}\exp\left(-\frac{4\pi}{3}\kappa\right) \ . \tag{12}$$

If scaling is complete, the scaling function should describe the behavior of branched-polymer-like vesicles, where $\langle V\rangle \sim N$, in the limit $y \to \infty$. We, therefore, expect

$$\Theta_V(y) \sim y^{-1} \tag{13}$$

for large y. Our results are shown in Fig. 5. The data follow the expected scaling behavior extremely well. The data for $\ell_0 = \sqrt{2.0}$ show a breakdown of scaling at small λ [44]. However, it has been shown in Ref. [40] for ring polymers that this is due to the "saturation" of the bending rigidity as $\lambda \to 0$. Scaling can be extended into this region through the use of nonlinear scaling fields [40]. The origin of an "intrinsic" bending rigidity is the use of hard spheres of finite radius to model self-avoiding membranes [45].

In fact, the same scaling ansatz for the volume of low-bending-rigidity vesicles has already been used in Ref. [9]. However, they employed the ratio N/κ as the scaling variable. A comparison of our Fig. 5 with Fig. 3 of Ref.

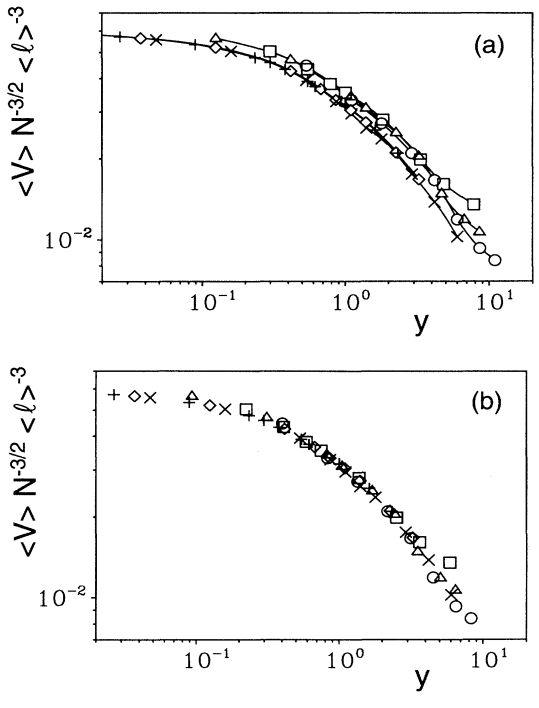

FIG. 5. The scaled volume $\langle V\rangle N^{-3/2}\langle \ell\rangle^{-3}$ for $p = 0$ as a function of the scaling variable $y = y_0(\ell_0)\sqrt{N}\exp[-4\pi\lambda/(3\sqrt{3})]$. Data are given for $\ell_0 = \sqrt{2.8}$, with $N = 127$ (+), $N = 247$ ($\diamond$), and $N = 407$ ($\times$), and for $\ell_0 = \sqrt{2.0}$, with $N = 127$ ($\square$), $N = 247$ ($\triangle$), and $N = 407$ ($\circ$). (a) $y_0(\ell_0) \equiv 1.0$, (b) $y_0(\sqrt{2.8}) \equiv 1.0$, and $y_0(\sqrt{2.0}) = 0.75$.

[9] shows that the data collapse is much better when the correct scaling variable (12) is used.

In summary, (i) the data scale for *all* values of κ, (ii) the persistence length we determine is in complete agreement with the result of field-theoretic renormalization group calculations [41–43], and (iii) for any fixed κ, sufficiently large vesicles exhibit branched-polymer scaling behavior. It follows that there is *no* phase transition at $p = 0$ for finite κ so that for large enough membrane size and fixed κ, vesicles are always crumpled.

V. SCALING BEHAVIOR FOR LARGE BENDING RIGIDITY κ

An analysis of vesicle shapes in the low-temperature limit [28] implies that the correct scaling variable in the large-κ regime is the reduced pressure $\tilde{p} = pV_{sphere}/\kappa \sim pN^{3/2}\kappa^{-1}$. Phase transitions should occur at $\tilde{p} = \text{const}$. The scaling behavior of both the discocyte-dumbbell transitions and the line of compressibility maxima for $p < 0$ are consistent with this prediction, see Fig. 6. The peak height χ_{max} of the compressibility along this line scales as $\chi_{max} \sim N^{-\gamma}$, with $\gamma = 1.35 \pm 0.05$ for $p < 0$, as shown in Fig. 7. This seems to imply that there is a continuous phase transition in the thermodynamic limit on crossing this line of compressibility maxima.

The scaling behavior of the volume and the asphericities in the prolate phase at large bending rigidities can be understood by considering the effective Gaussian Hamiltonian

$$\mathcal{H}_{eff}/(k_BT) = \int d^2r \tfrac{1}{2}\left[\kappa(\nabla^2 u)^2 + \sigma(\nabla u)^2\right] \qquad (14)$$

for the undulations of an almost flat membrane with a surface tension σ. Here, $u(\mathbf{r})$ measures the deviations of the membrane positions from a flat reference state. For a membrane of linear lateral extension L, the mean-square amplitude of fluctuations is

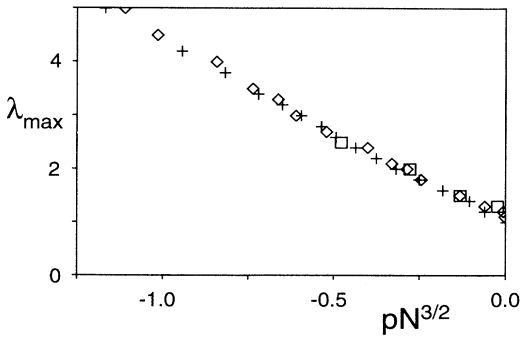

FIG. 6. The location λ_{max} of the maximum in the compressibility as a function of the scaled pressure $pN^{3/2}$ for $p < 0$. Data are given for $\ell_0 = \sqrt{2.8}$ and $N = 127$ (+), $N = 247$ (◇), and $N = 407$ (□).

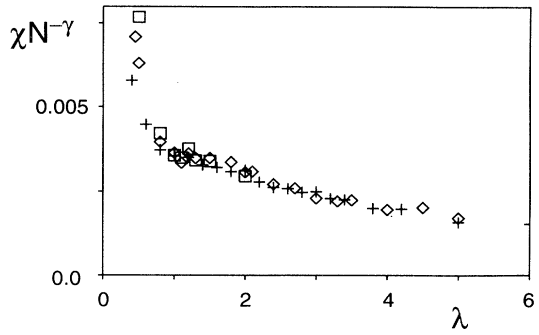

FIG. 7. The scaled peak compressibility $\chi_{max}N^{-\gamma}$ with $\gamma = 1.35 \pm 0.05$, as a function of the bending rigidity λ. Data are given for $\ell_0 = \sqrt{2.8}$ and $N = 127$ (+), $N = 247$ (◇), and $N = 407$ (□).

$$\langle u^2\rangle = \int \frac{d^2k}{(2\pi)^2}\frac{1}{\kappa k^4 + \sigma k^2} = \frac{1}{4\pi\sigma}\ln\left(1 + \frac{1}{4\pi^2}\frac{\sigma}{\kappa}L^2\right) . \qquad (15)$$

We now use the Laplace equation to relate the surface tension σ of a vesicle of radius R to the pressure increment p,

$$p = \frac{2\sigma}{R} . \qquad (16)$$

The area of an inflated vesicle is $4\pi R^2 \simeq 2(N-2)\langle\ell\rangle^2\sqrt{3}/4$, so that

$$R \simeq 3^{-1/4}2^{-3/2}\pi^{-1/2}\langle\ell\rangle\sqrt{N-2} . \qquad (17)$$

With $L^2 = 4\pi R^2$, we finally arrive at

$$\langle u^2\rangle = \frac{1}{2\pi pR}\ln\left(1 + \beta\frac{pR^3}{\kappa}\right) , \qquad (18)$$

where $\beta = 1/(2\pi) \simeq 0.159$. For a vesicle that is ellipsoidal on average, the volume can be estimated to be

$$\langle V\rangle \simeq \frac{4\pi}{3}\left(R - \alpha_1\sqrt{\langle u^2\rangle}\right)\left(R - \alpha_2\sqrt{\langle u^2\rangle}\right) \times \left(R - \alpha_3\sqrt{\langle u^2\rangle}\right) = \frac{4\pi}{3}R^2\left[R - (\alpha_1+\alpha_2+\alpha_3)\sqrt{\langle u^2\rangle} + O(1/R)\right] . \qquad (19)$$

Thus, for shapes that deviatiate not too stongly from a sphere, we have

$$\langle V\rangle \simeq \frac{4\pi}{3}R^2\left[R - \alpha\sqrt{\frac{1}{2\pi pR}\ln\left(1 + \beta\frac{pR^3}{\kappa}\right)}\right] . \qquad (20)$$

Since we have made several approximations in the derivation of Eq. (20), we use not only $\alpha \equiv (\alpha_1 + \alpha_2 + \alpha_3)$ but also β as adjustable parameters when comparing with the Monte Carlo data.

Similarly, the asphericities $\Gamma_1 \equiv \langle \Lambda_1/\Lambda_3 \rangle$ and $\Gamma_2 \equiv \langle \Lambda_2/\Lambda_3 \rangle$ should be given by

$$\Gamma_i \simeq \frac{R - \alpha_i\sqrt{\langle u^2 \rangle}}{R - \alpha_3\sqrt{\langle u^2 \rangle}} \simeq 1 - (\alpha_i - \alpha_3)\sqrt{\langle u^2 \rangle}/R \qquad (21)$$

so that

$$\Gamma_i \simeq 1 - (\alpha_i - \alpha_3)\sqrt{\frac{1}{2\pi p R^3} \ln\left(1 + \beta\frac{pR^3}{\kappa}\right)} \; . \qquad (22)$$

The most important contribution to the integral (15) comes from the long wavelength modes. These modes are controlled by the *renormalized* bending rigidity [41–43]

$$\kappa_R(R) = \kappa - \frac{3}{4\pi} \ln(R/a_0) \; , \qquad (23)$$

where a_0 is of the order of the tether length ℓ_0. Thus, κ in Eqs. (20) and (22) should be replaced by $\kappa_R(R)$. The renormalization of σ and the effect of a finite σ on the renormalization of κ can be neglected for $R^2 < \sqrt{\kappa/|\sigma|}$ [46], which is just the regime we are interested in [47].

The result (20) shows that the maximum in the compressibility is due to a *buckling* transition of a finite membrane which occurs for $p < 0$ and $|p| \nearrow \kappa/\beta R^3$. When the renormalization of κ is neglected, the transition pressure scales as $pN^{3/2}/\kappa$, as observed above. The renormalization of κ gives only a weak logarithmic correction to this scaling behavior. A comparison of (20) with the Monte Carlo data for two different system sizes is shown in Fig. 8. Here, the coefficient β has been determined by the requirement that $\langle u^2 \rangle$, Eq. (18), diverges at the position of the peak in the compressibility. Both the shape of the curves and the finite size behavior are in good agreement with our data.

In order to understand in more detail the behavior of the volume and of the compressibility in the vicinity of the buckling transition, we have to include the effect of the entropic repulsion [48] between segments of the membrane on opposite sides of the vesicle. This can be done in an approximate fashion by adding an effective potential [49] to the Hamiltonian (14) which describes the fluctuations of a membrane between two planar walls of separation $2d$,

$$\mathcal{H}_{eff}/(k_BT) = \int d^2r \tfrac{1}{2}\kappa \left[(\nabla^2 u)^2 + \frac{\sigma}{\kappa}(\nabla u)^2 + \xi_\parallel^{-4} u^2\right] \; . \qquad (24)$$

In the vicinity of the buckling transition, the condition

$$\langle u^2 \rangle = \mu d^2 \qquad (25)$$

with a constant $\mu \simeq 1/6$ [48] implies

$$4\xi_\parallel^{-4} \simeq \left(\frac{1}{4\pi\kappa\mu d^2}\right)^2 + \left(\frac{\sigma}{\kappa}\right)^2 \; . \qquad (26)$$

We can now proceed as before and calculate $\langle u^2 \rangle$ for a finite piece of membrane of linear extension L:

$$\langle u^2 \rangle = \tfrac{1}{2}\mu d^2 \left\{1 - \frac{2}{\pi} \arctan\left[\left(8\pi^2 + \frac{\sigma}{\kappa}L^2\right) 4\pi\kappa\mu \frac{d^2}{L^2}\right]\right\} \; . \qquad (27)$$

For a vesicle, we identify $L^2 = 4\pi R^2$, $\sigma = pR/2$, and $d = R$, so that

$$\langle u^2 \rangle = \tfrac{1}{2}\mu R^2 \left\{1 - \frac{2}{\pi} \arctan\left[\left(4\pi + \frac{pR^3}{\kappa}\right) 2\pi\kappa\mu\right]\right\} . \qquad (28)$$

This result can then be inserted into Eq. (19) to determine the volume. The compressibility (6) is then easily calculated to be

$$\chi = R^3 F(pR^3, \kappa) \; , \qquad (29)$$

with

$$F(pR^3,\kappa) = \sqrt{2}\alpha\mu^{3/2}\Big\{\left[1 - \alpha\sqrt{\mu/2} f(pR^3,\kappa)\right] f(pR^3,\kappa) \times \left[1 + g(pR^3,\kappa)^2\right]\Big\}^{-1} \; , \qquad (30)$$

where

$$f(pR^3,\kappa) = 1 - \frac{2}{\pi} \arctan\left(g(pR^3,\kappa)\right) \qquad (31)$$

and

$$g(pR^3,\kappa) = 2\pi\mu\left(4\pi\kappa + pR^3\right) \; . \qquad (32)$$

In this result, κ should again be replaced by the renormalized quantity $\kappa_R(R)$.

If the renormalization of κ is ignored, the scaling form (29) immediately implies

$$\chi_{max} \sim N^{3/2}, \qquad (33)$$

or $\gamma = 1.5$. The renormalization of κ, Eq. (23), gives an additional logarithmic correction to this scaling behavior.

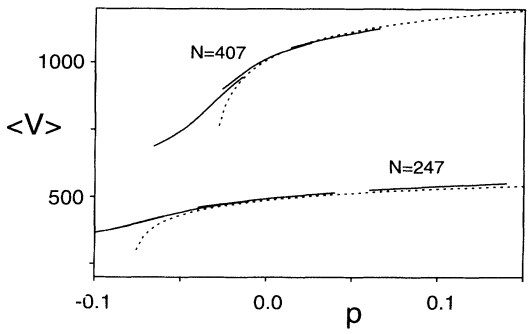

FIG. 8. The average volume $\langle V \rangle$ as a function of the pressure p for $\lambda = 2.0$. The full lines are the Monte Carlo data for $N = 247$ and $N = 407$, with $\ell_0 = \sqrt{2.8}$. The dashed lines are the result of the approximation (20), with $\alpha = 2.73$ and $\beta = 0.038$.

Since the Monte Carlo data are certainly affected by corrections to scaling, we believe that (33) is in reasonable agreement with our simulation results.

VI. SCALING BEHAVIOR FOR SMALL BENDING RIGIDITY κ

The scaling behavior in the small-κ portion of the phase diagram is different. We have argued in Ref. [11] that, for $\lambda = 0$, the crumpled-to-inflated transition occurs at $\overline{p} = pN^{\zeta} = \text{const}$, with $\zeta = 1/2$. This is consistent with the data presented in Ref. [11] when a "shift variable" N_0 is introduced to account for the leading corrections to scaling [38], so that $\overline{p} = p(N-N_0)^{\zeta}$. We find here that this scaling behavior holds not only for $\lambda = 0$, but along the whole line of first-order crumpled-to-inflated transitions, see Fig. 9(a). Furthermore, data taken along the line of compressibility maxima for $\lambda < 1.0$ also scale in this way. When no shift variable is used, our data scale best with $\zeta = 0.65 \pm 0.05$, as shown in Fig. 9(b). For $\lambda = 0$, this value ζ is in agreement with the result of Ref. [12]. With the present range of vesicle sizes, however, it is not possible to distinguish between these two estimates for ζ.

In the inflated phase, for $\lambda = 0$, the volume was found in Ref. [11] to scale as

$$\langle V \rangle = V_0 p^{3\omega} N^{3\nu_+}, \tag{34}$$

where

$$\omega = \frac{1-\nu}{3\nu-1} \quad , \quad \nu_+ = \frac{\nu}{3\nu-1} \tag{35}$$

with an exponent $\nu \simeq 0.79$, so that $3\omega = 0.47 \pm 0.01$ and $3\nu_+ = 1.735 \pm 0.005$. We have, therefore, calculated $\langle V \rangle$ and χ as a function of p in the inflated phase, for $\lambda = 0.50$ and $\lambda = 1.0$, with vesicle sizes $N = 247$ and $N = 407$. The results obtained using the Ferrenberg-Swendsen reweighting technique [50] are shown in Figs. 10 and 11. For $\lambda = 0.50$, we find that $3\omega = 0.42 \pm 0.02$ and $3\nu_+ = 1.718 \pm 0.010$, in agreement with Eq. (35). Accounting for the fact that the range of pressures for which the data scale decreases with increasing λ, we believe that these values for ω and ν_+ are consistent with those obtained for $\lambda = 0$. Our results, therefore, support the conclusion that the scaling behavior in the inflated phase near the line of crumpled-to-inflated transitions is described by a single, universal exponent $\nu \simeq 0.79$. For $\lambda = 1.0$, we find $3\omega = 0.265 \pm 0.02$ and $3\nu_+ = 1.653 \pm 0.010$, which is considerably smaller than the values obtained at smaller λ [but still consistent with the scaling relation $2\nu_+ = 1 + \omega$ implied by Eq. (35)]. However, data taken for this value of λ probably lie outside the small-κ scaling regime.

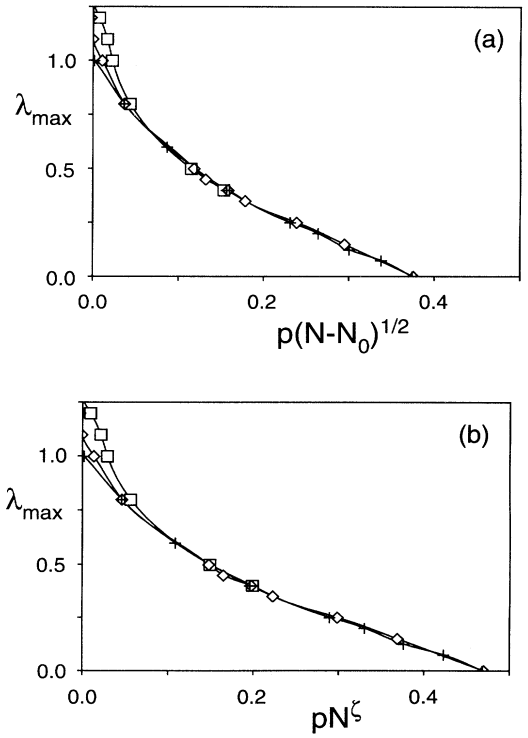

FIG. 9. The location λ_{max} of the maximum in the compressibility as a function of the scaled pressure for $p > 0$. (a) $p(N - N_0)^{1/2}$, with $N_0 = 40$; (b) pN^{ζ}, with $\zeta = 0.65$. Data are given for $\ell_0 = \sqrt{2.8}$ and $N = 127$ (+), $N = 247$ ($\diamond$), and $N = 407$ ($\square$).

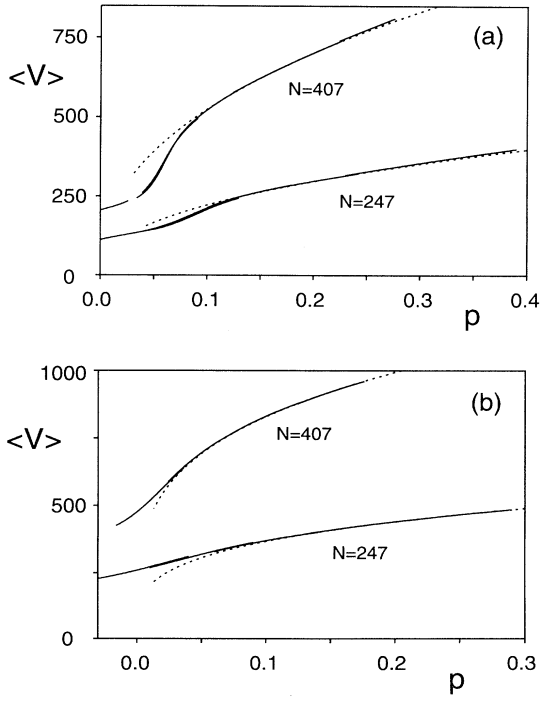

FIG. 10. The average volume $\langle V \rangle$ as a function of the pressure increment p for $N = 247$ and $N = 407$, with (a) $\lambda = 0.50$ and (b) $\lambda = 1.0$. The Monte Carlo data are shown as full lines. The dashed lines indicate the power law behavior $\langle V \rangle = V_0 p^{3\omega} N^{3(1+\omega)/2}$ with (a) $3\omega = 0.42$ and $V_0 = 0.047\,48$, and (b) $3\omega = 0.26$ and $V_0 = 0.084\,14$.

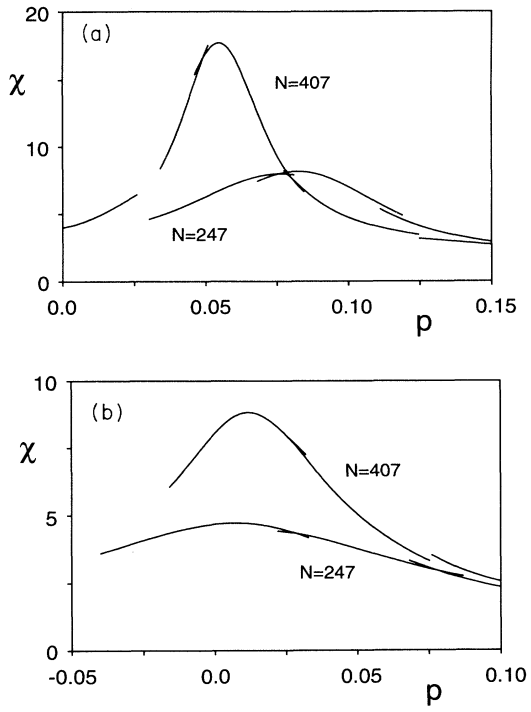

FIG. 11. The compressibility χ as a function of the pressure increment p for $N = 247$ (dashed lines) and $N = 407$ (full lines), with (a) $\lambda = 0.50$ and (b) $\lambda = 1.0$.

VII. THE TRANSITION FROM STOMATOCYTES TO BRANCHED POLYMERS

Finally, a rough estimate for the location of the line of transitions from stomatocytes to crumpled configurations can be obtained as follows. Assume that the branched-polymer-like configurations consist of thin cylindrical arms of radius ξ. The free energy can then be approximated as

$$\mathcal{F}_{bp}/(k_BT) = -M\ln(z) + \tfrac{3}{2}\ln(M) - p\langle V\rangle + \tfrac{1}{2}\kappa\left\langle \int_A dA(c_1+c_2)^2 \right\rangle + \bar{\kappa}\left\langle \int_A dA c_1 c_2 \right\rangle, \tag{36}$$

where $A \sim N$ is the surface area, c_1 and c_2 are the local principal curvatures, z is a N-independent constant, and $M = A/2\pi\xi^2$ is the equivalent number of "monomers" of a branched polymer. The first two terms in Eq. (36) are the branched-polymer entropy [51], while the last two terms are the average bending energy and the average Gaussian curvature. The average volume is $\langle V\rangle \simeq A\xi/2$. The bending energy is estimated to be $\kappa_R(\xi)A\xi^{-2}/2$, where

$$\kappa_R(\xi) = \kappa - \frac{3}{4\pi}\ln(\xi/a_0) \tag{37}$$

is the renormalized bending rigidity [41] at length scale ξ. Here, a_0 is of the order of the tether length ℓ_0. Due to the Gauss-Bonnet theorem, the integral over the Gaussian curvature is a topological invariant, 4π. However, the renormalization of the saddle-splay modulus [43,52]

$$\bar{\kappa}_R(\xi) = \bar{\kappa} + \frac{5}{6\pi}\ln(\xi/a_0) \tag{38}$$

has to be taken into account. There are additional logarithmic contributions to the free energy which are due to the suppression of translational zero modes [53]. However, because they are identical in both the branched-polymer and stomatocyte phases, they can be neglected when determining the phase transition line. Since the surface area is held constant, the only variable in $\mathcal{F}_{bp}$ is the arm radius ξ, which is determined by minimizing the free energy.

For the stomatocyte, the renormalization of the bending elasticity is a two-step process. For length scales smaller than the parallel correlation length $\xi_\parallel \sim \sqrt{\kappa d}$ [54], the two shells of the stomatocyte fluctuate almost independently so that at length scale $\xi_\parallel$ the renormalized rigidities of the two shells are $\kappa_R(\xi_\parallel)$ and $\bar{\kappa}_R(\xi_\parallel)$. Since $\xi_\parallel$ is of the order of the tether length in the simulations, this renormalization is a small effect which we ignore in our analysis. For larger length scales, the two shells of the stomatocyte fluctuate together, as a "double layer," with bare bending rigidity $2\kappa_R(\xi_\parallel)$. A similar argument can be made for the saddle-splay modulus. However, due to the presence of the neck, the bare value is now $\bar{\kappa}$, so that one arrives at the usual renormalized value $\bar{\kappa}_R(R)$ (if the contribution of length scales less than $\xi_\parallel$ is again neglected). The free energy of a stomatocyte of radius R is, therefore, estimated to be

$$\mathcal{F}_{stom}/(k_BT) = 8\pi\kappa_R^{(2)}(R) + 4\pi\bar{\kappa}_R(R) + f_{neck} - p\langle V\rangle + c_\infty\frac{A}{\kappa}d^{-2}, \tag{39}$$

where the first term is the average bending energy of the inner and the outer shells of the stomatocyte, with $R^2 = A/(8\pi)$ and

$$\kappa_R^{(2)}(R) = 2\kappa_R(\xi_\parallel) - \frac{3}{4\pi}\ln(R/\xi_\parallel)\ , \tag{40}$$

the second term is the average Gaussian curvature contribution, the third (constant) term the bending energy of the neck region, and the last term the steric repulsion [48] between the two shells at distance d, with an amplitude c_∞. This approximation should be valid for d much smaller than the vesicle radius R. For small necks, the energy of the neck region almost vanishes for the curvature Hamiltonian (1), since the neck is almost a minimal surface. However, in the triangulated surface model, the angle between neighboring triangles becomes very large in the neck, so that the neck cannot be described by the continuum model (1). f_{neck} is thus the contribution of the nonlinear bending elasticity.

The average volume is estimated to be $\langle V\rangle = Ad$. A self-consistent calculation of the free energy of the lamellar phase gives $c_\infty = 3\pi^2/128 = 0.231$ [48], while Monte Carlo simulations predict $c_\infty = 0.106$ [55,56]. The only

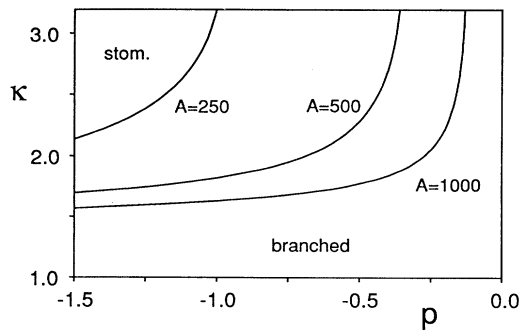

FIG. 12. The line of phase transitions between stomatocytes and the branched-polymer phase calculated using (36) and (39), with $\bar{\kappa} = -\kappa$, $c_\infty = 0.1$, $z = 20$, and $f_{neck} = \kappa$.

variable in Eq. (39) is the distance d, which is again calculated by minimizing the free energy, so that

$$d^3 = \frac{2c_\infty}{(-p)\kappa} . \tag{41}$$

The resulting estimate for the stomatocyte free energy is

$$\mathcal{F}_{stom}/(k_BT) = 2 \times 8\pi\kappa_R(R) + 4\pi\bar{\kappa}_R(R) + f_{neck} + \frac{3}{2}\left(\frac{2c_\infty}{\kappa}\right)^{1/3} A(-p)^{2/3} . \tag{42}$$

The results for the location of transitions from stomatocytes to crumpled configurations obtained using these approximations are shown in Fig. 12. The main features seen in Fig. 1 are reproduced. The transition line shifts to lower values of κ with increasing N; simultaneously its pressure dependence becomes weaker. The analysis also indicates that a limiting form of the transition line is reached rather quickly with increasing system size, so that our Monte Carlo results for $N = 247$ can be expected to be close to the thermodynamic limit.

VIII. SUMMARY AND CONCLUSIONS

In this paper we have studied the behavior of fluid vesicles as a function of the bending rigidity κ and the pressure increment p. We have presented evidence that there is no phase transition separating distinct large-bending-rigidity and crumpled phases at $p = 0$ when the bending rigidity is varied. Instead, it has been found that the scaling behavior for all κ is determined by a single length scale, the persistence length ξ_p. Our data confirm the exponential dependence of ξ_p on κ which has been calculated using a field-theoretic renormalization group approach. Phase transitions do occur, however, between branched-polymer and inflated shapes at small κ and $p > 0$, and between stomatocytes and branched-polymer or prolate shapes for sufficiently large κ and $p < 0$.

Several open questions remain. First, it would be nice if the absence of a phase transition at $p = 0$ could be confirmed by simulations of larger vesicle sizes. It has been shown in Ref. [16] that without self-avoidance, vesicles of size $N < 1000$ can be simulated with reasonable accuracy. The simulations with self-avoidance are more time consuming, but should be tractable for $N \simeq 1000$ with available machines. Second, the line of phase transitions between branched-polymer and inflated shapes should be studied in more detail. In particular, the nature of the critical point, and the scaling behavior, have to be determined. It would also be interesting to know whether the scaled critical pressure $p_c N^\zeta$ stays finite or approaches zero for $N \to \infty$. Furthermore, it is necessary to understand the behavior near the line of susceptibility maxima in the region $p \simeq 0$. This should lead to more insight into the excitations that cause the peak in the specific heat discussed in Sec. IV.

Finally, it would be very useful if these results could be compared with experiments on low-bending-rigidity vesicles. It seems that the best possibility for obtaining large vesicles with bending rigidities of order k_BT, which are stable on experimental time scales, is to use mixtures of either a lipid with a short-chain amphiphile [57] or of two lipids with different spontaneous curvatures [58–60]. Mixtures have the additional advantage that the value of κ can be tuned by changing the composition of the membrane [57–60]. Indeed, the only current experiments with low-bending-rigidity vesicles have utilized these methods [21,61].

ACKNOWLEDGMENTS

This work was supported in part by the Deutsche Forschungsgemeinschaft through Sonderforschungsbereich 266, the donors of The Petroleum Research Fund, administered by the ACS, the University of Minnesota Army High Performance Computing Research Center, U.S. Army Contract No. DAAL03-89-C-0038, and NATO Grant No. CRG910156.

[1] *Statistical Mechanics of Membranes and Surfaces*, edited by D.R. Nelson, T. Piran, and S. Weinberg (World Scientific, Singapore, 1989).
[2] R. Lipowsky, Nature **349**, 475 (1991).
[3] M. Bloom, E. Evans, and O.G. Mouritsen, Q. Rev. Biophys. **24**, 293 (1991).
[4] P.B. Canham, J. Theor. Biol. **26**, 61 (1970).
[5] W. Helfrich, Z. Naturforsch. **28c**, 693 (1973); H.J. Deuling and W. Helfrich, J. Phys. (Paris) **37**, 1335 (1976).
[6] E. Evans, Biophys. J. **14**, 923 (1974).
[7] M. Wortis, U. Seifert, K. Berndl, B. Fourcade, L. Miao, M. Rao, and R.K.P. Zia, in *Dynamical Phenomena at Interfaces, Surfaces and Membranes*, edited by D. Beysens, N. Boccara, and G. Forgacs (Nova Science, New York, 1993).
[8] D.M. Kroll and G. Gompper, Science **255**, 968 (1992).

[9] D. Boal and M. Rao, Phys. Rev. A **45**, R6947 (1992).
[10] A. Baumgärtner, Physica A **192**, 550 (1993).
[11] G. Gompper and D.M. Kroll, Europhys. Lett. **19**, 581 (1992); Phys. Rev. A **46**, 7466 (1992).
[12] B. Dammann, H.C. Fogedby, J.H. Ipsen, and C. Jeppesen, J. Phys. (France) I **4**, 1139 (1994).
[13] A. Baumgärtner, Physica A **190**, 63 (1992).
[14] A. Baumgärtner, J. Chem. Phys. **98**, 7496 (1993).
[15] In Refs. [10,13,14] a plaquette model on a simple cubic lattice is used to study the membrane fluctuations of vesicles.
[16] M. Bowick, P. Coddington, L. Han, G. Harris, and E. Marinari, Nucl. Phys. B **394** (1993); K. Anagnostopoulos, M. Bowick, P. Coddington, M. Falconi, L. Han, G. Harris, and E. Marinari, Phys. Lett. B **317**, 102 (1993).
[17] J. Ambjørn, A. Irbäck, J. Jurkiewicz, and B. Petersson, Nucl. Phys. B **393**, 571 (1993).
[18] The simulations of Refs. [16,17] are for surfaces *without* self-avoidance.
[19] D.M. Kroll and G. Gompper, Phys. Rev. A **46**, 3119 (1992).
[20] C.F. Baillie and D.A. Johnston, Phys. Lett. B **283**, 55 (1992).
[21] G. Cevc and G. Blume, Biochim. Biophys. Acta **1104**, 226 (1992).
[22] A. Billoire and F. David, Nucl. Phys. B **275**, 617 (1986); D.V. Boulatov, V.A. Kazakov, I.K. Kostov, and A.A. Migdal, *ibid.* **275**, 641 (1986).
[23] J.-S. Ho and A. Baumgärtner, Europhys. Lett. **12**, 295 (1990); A. Baumgärtner and J.-S. Ho, Phys. Rev. A **41**, 5747 (1990).
[24] Y. Kantor and D.R. Nelson, Phys. Rev. Lett. **58**, 2774 (1987).
[25] H.S. Seung and D.R. Nelson, Phys. Rev. A **38**, 1005 (1988).
[26] $\langle \ell \rangle$ differs by only a few percent in various portions of the phase diagram.
[27] U. Seifert and R. Lipowsky, Phys. Rev. A **42**, 4768 (1990).
[28] K. Berndl, J. Käs, R. Lipowsky, E. Sackmann, and U. Seifert, Europhys. Lett. **13**, 659 (1990); U. Seifert, K. Berndl, and R. Lipowsky, Phys. Rev. A **44**, 1182 (1991).
[29] We thank R. Lipowsky and U. Seifert for pointing this out.
[30] S.M. Catterall, Phys. Lett. B **220**, 207 (1989).
[31] C.F. Baillie, D.A. Johnston, and R.D. Williams, Nucl. Phys. B **335**, 469 (1990).
[32] C.F. Baillie, R.D. Williams, S.M. Catterall, and D.A. Johnston, Nucl. Phys. B **348**, 543 (1991).
[33] R.L. Renken and J.B. Kogut, Nucl. Phys. B **354**, 328 (1991).
[34] S.M. Catterall, D. Eisenstein, J.B. Kogut, and R.L. Renken, Nucl. Phys. B **366**, 647 (1991).
[35] C. Münkel and D.W. Heermann, J. Phys. (France) I **3**, 1359 (1993).
[36] P.-G. de Gennes and C. Taupin, J. Phys. Chem. **86**, 2294 (1982).
[37] S. Leibler, R.R.P. Singh, and M.E. Fisher, Phys. Rev. Lett. **59**, 1989 (1987).
[38] C.J. Camacho and M.E. Fisher, Phys. Rev. Lett. **65**, 9 (1990).
[39] A.C. Maggs, S. Leibler, M.E. Fisher, and C.J. Camacho, Phys. Rev. A **42**, 691 (1990).
[40] C.J. Camacho, M.E. Fisher, and R.R.P. Singh, J. Chem. Phys. **94**, 5693 (1991).
[41] L. Peliti and S. Leibler, Phys. Rev. Lett. **54**, 1690 (1985).
[42] D. Förster, Phys. Lett. A **114**, 115 (1986).
[43] H. Kleinert, Phys. Lett. A **114**, 263 (1986).
[44] For $\ell_0 = \sqrt{2.8}$ the membrane is not completely self-avoiding for small λ. We only show data for $\ell_0 = \sqrt{2.8}$ in Fig. 5, which are unaffected by self-intersections.
[45] F.F. Abraham and D.R. Nelson, J. Phys. (France) **51**, 2653 (1990).
[46] F. David and S. Leibler, J. Phys. (France) II **1**, 959 (1991).
[47] We assume here that the result obtained in Ref. [46] for $\sigma > 0$ also holds for $\sigma < 0$.
[48] W. Helfrich, Z. Naturforsch. **33a**, 305 (1978).
[49] R. Lipowsky, Europhys. Lett. **7**, 255 (1988).
[50] A.M. Ferrenberg and R.H. Swendsen, Phys. Rev. Lett. **61**, 2635 (1988).
[51] G. Parisi and N. Sourlas, Phys. Rev. Lett. **46**, 871 (1981).
[52] F. David, in *Statistical Mechanics of Membranes and Surfaces* (Ref. [1]).
[53] D.C. Morse and S.T. Milner, Europhys. Lett. **26**, 565 (1994).
[54] F. Brochard and J.F. Lennon, J. Phys. (Paris) **36**, 1035 (1975).
[55] G. Gompper and D.M. Kroll, Europhys. Lett. **9**, 59 (1989).
[56] W. Janke, H. Kleinert, and M. Meinhard, Phys. Lett. B **217**, 525 (1989).
[57] M.M. Kozlov and W. Helfrich, Langmuir **8**, 2792 (1992).
[58] S. Leibler and D. Andelman, J. Phys. (Paris) **48**, 2013 (1987).
[59] S.A. Safran, P. Pincus, and D. Andelman, Science **248**, 354 (1990).
[60] U. Seifert, Phys. Rev. Lett. **70**, 1335 (1993).
[61] H.P. Duwe, J. Käs, and E. Sackmann, J. Phys. (Paris) **51**, 945 (1990).